Geotextiles and Geomembranes 47 (2019) 632–641

Contents lists available at ScienceDirect

Geotextiles and Geomembranes

journal homepage: www.elsevier.com/locate/geotexmem

Large-scale load capacity tests on a geosynthetic encased column

Nima R. Alkhorshid[a,*], Gregório L.S. Araujo[b], Ennio M. Palmeira[b], Jorge G. Zornberg[c]

[a] Federal University of Itajubá, Institute of Integrated Engineering, 35903-087, Itabira, MG, Brazil
[b] University of Brasília, Department of Civil and Environmental Engineering, 70910-900, Brasília, DF, Brazil
[c] The University of Texas at Austin, Civil, Architectural and Environmental Engineering Department, Austin, TX, 78712, USA

ARTICLE INFO

Keywords:
Geosynthetics
Embankment
Soft soil
Geotextile
Large-scale test
Encased column

ABSTRACT

Stone columns have been used to minimize the settlement of embankments on soft soils but their use in very soft soils can become challenging, partly because of the low confinement provided by the surrounding soil. Geosynthetic encased columns (GECs) have been successfully used to enhance to reduce settlements of embankments on soft soils. This paper describes an investigation on the performance of encased columns constructed on a very soft soil using different types of encasement (three woven geotextiles with different values of tensile stiffness) and different column fill materials (sand, gravel and recycled construction and demolition waste, RCDW). The results of load capacity tests conducted on large-scale models constructed to simulate the different types of GECs indicate that the displacement method adopted during column installation can lead to an enhanced shear strength in the smear zone that develops within the very soft soil. In addition, breakage of the column fill material was found to affect the load-settlement response of gravel and RCDW columns. Furthermore, the excess pore water pressure generated in the surrounding soil during installation, was found to remain limited to radial distances smaller than three times the GEC diameter.

1. Introduction

The stone column method is among the most efficient improvement techniques for soft foundation soils, both in terms of cost and installation time. This method has been extensively used in projects involving embankments founded on soft soils, with columns generally containing sand or gravel. Use of granular infill also provides horizontal drainage to expedite consolidation of the soft soil and to support a significant fraction of the embankment weight. Since the column fill material often involves aggregates of comparatively large particle size, the lateral confinement provided by the surrounding soil is of the utmost importance for its performance. However, for projects involving very soft soils (e.g. undrained shear strength, S_u below 15 kPa), the particularly low lateral confinement acting on the stone column may lead to significant internal stability challenges. In addition, performance aspects related to the possible migration of fine particles into the aggregate fill material, and associated clogging, must be taken into consideration. To overcome these limitations, the column granular materials can be encased using a geotextile layer, which can provide confinement of the aggregate infill and also serve as filter. Applying axial load on the column material will result in lateral deformations of the infill aggregate and mobilization of tensile forces in the encasement. The confinement of the granular infill resulting from mobilization of encasement tensile forces is the primary difference between geosynthetic encased columns (GECs) and conventional granular columns.

The performance of GECs has been evaluated in previous studies through laboratory tests, analytical studies and numerical simulations, and field evaluations. Laboratory and field tests have largely focused on the deformation of columns under loading, considering conventional columns as well as partial or full encasement of columns in soft and collapsible soils (Murugesan and Rajagopal, 2007; Gniel and Bouazza, 2009; Murugesan and Rajagopal, 2009; Araujo et al., 2009; McCabe et al., 2009; Cimentada et al., 2011; Ali et al., 2012, 2014; Dash and Bora, 2013; Ghazavi and Afshar, 2013; Miranda et al., 2015; Noor Muneerah PG Haji Jeludin et al., 2015; Xu et al., 2016; Gu et al., 2016; Hong et al., 2016; Rayamajhi et al., 2016; Fattah et al., 2016; Ou Yang et al., 2017; Geng et al., 2017; Mazumder et al., 2018; Xue et al., 2019).

Analytical studies have been conducted on the performance of encased and conventional columns considering the evaluation of unit cells. Most of these studies have assumed that settlements of the column and the surrounding soil are the same, and have adopted either elastic or elastoplastic models for the column fill material (Raithel and Kempfert, 2000; Zhang et al., 2011; Pulko et al., 2011; Castro and Sagaseta, 2011). Briaud (2013) presented an analytical method to

* Corresponding author.
E-mail addresses: nimara@unifei.edu.br (N.R. Alkhorshid), gregorio@unb.br (G.L.S. Araujo), palmeira@unb.br (E.M. Palmeira), zornberg@mail.utexas.edu (J.G. Zornberg).

https://doi.org/10.1016/j.geotexmem.2019.103458

Available online 06 June 2019

predict the load bearing capacity of a single encased column. This method takes into account the influence of the geosynthetic tensile stiffness and the elevation of the water table to estimate the load capacity of the column.

The behavior of a single or a group of encased and conventional columns has also been assessed via numerical simulations. Chen et al. (2015) presented laboratory tests and numerical simulations of an embankment supported by geosynthetic-encased columns, the results of which showed that the failure of encased columns was governed by column bending. Numerical evaluations have also been carried out to simulate the behavior of encased columns (Khabbazian et al., 2010; Alkhorshid, 2012; Kaliakin et al., 2012; Keykhosropur et al., 2012; Elsawy, 2013; Almeida et al., 2013; Alkhorshid et al., 2014, 2018; Shahu, and Reddy, 2014; Hosseinpour et al., 2015; Mohapatra et al., 2017; Rajesh, 2017).

Alexiew and Raithel (2015) provided information on a number of projects in which encased columns were adopted as a ground improvement technique. This solution was reported to result in an accelerated consolidation process, as most of the settlement occurred during construction of the embankment. The authors also reported that excess pore water pressures were found to dissipate during construction under increments of surface loads and that column installation resulted in an increased undrained shear strength of the surrounding soil.

GECs have been used successfully in a number of projects (Raithel and Kempfert, 2000; Raithel et al., 2002; De Mello et al., 2008; Alexiew and Raithel, 2015; Schnaid et al., 2017). Design procedures have limitations because of their use of simplifying assumptions, including the hypothesis that settlements of the encased column equal those of the surrounding soil as well as the use of a constant stiffness value to represent the geotextile deformations. However, the design procedures have been reported to adequately predict the behavior of GECs (Raithel and Kempfert, 2000; Pulko et al., 2011). Consequently, a better understanding of the influence of encasement on the behavior of the column is needed to achieve robust design procedures. This paper aimed at investigating the behavior of an isolated geotextile encased granular column under laboratory controlled conditions. The experimental methodology, which involved construction of large-scale encased and non-encased models, as well as the results gathered during their installation and subsequent load capacity testing, are presented and discussed in the following sections.

2. Equipment and materials

2.1. Equipment

Fig. 1 shows the equipment used in the load capacity tests, which included a tank, measuring 1600 mm × 1600 mm x 1200 mm, with a reaction frame to facilitate application of the vertical load on the column.

Six piezometers (P1, P2, P3, P4, P5 and P6) were utilized to monitor the excess pore water pressure generated during the construction and loading phases. Additionally, three pressure cells (PC1, PC2 and PC3) were installed at the side of the column to measure lateral earth pressures around the column. Four displacement transducers and a load cell were used to measure displacements and loads at the top of the column. Fig. 1 shows the position of the different instruments used during load capacity testing. Additional information is provided by Alkhorshid (2017).

2.2. Materials

A slurry was prepared by mixing with water a locally available fine-grained soil, which was used to produce the soft soil layer used in the testing program. The particle size distribution of the fine-grained soil is presented in Fig. 2, and its properties are listed in Table 1. Bentonite (4% in mass) was added to the locally available soil to increase its

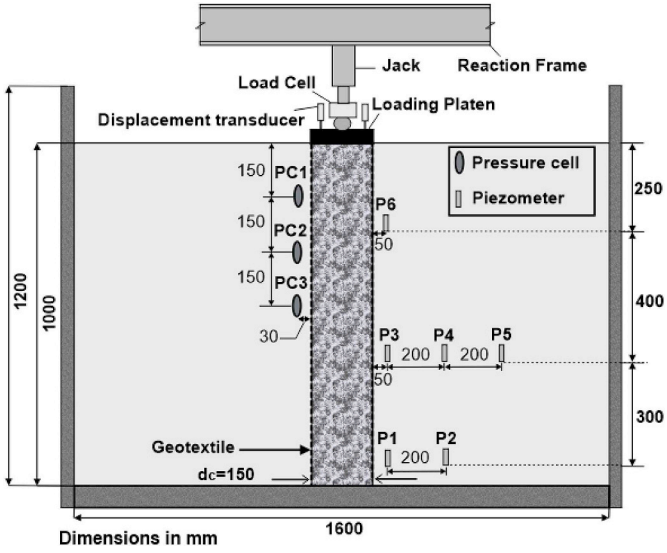

Fig. 1. Schematic of the setup for load capacity test on GEC.

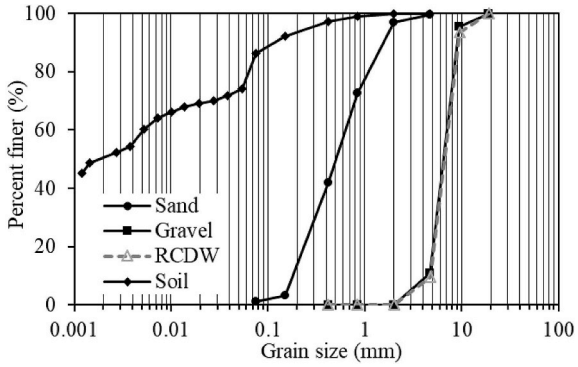

Fig. 2. Particle size distributions of the materials.

Table 1
Soft soil properties.

Soil properties	Value
w_L (%)	60
I_P (%)	21
G_s (−)	2.7
e (−)	1.23
C_c	0.47
C_s	0.03

Note: w_L = liquid limit; I_P = plasticity index; G_s = specific gravity; e = void ratio; C_c = compression index; C_s = swelling index.

plasticity and workability, resulting in the soft soil used throughout the testing program. Based on the Unified Soil Classification system (USCS), the soil is classified as C.H.

The hydraulic conductivity of the soil was found to be 4.2×10^{-5} cm/s, obtained in accordance with the recommendations of Brazilian standard NBR-14545/ABNT (2000) which is equivalent to ASTM D5084. To account for the scale differences between the laboratory models and typical full-scale prototype GECs, the values presented in Table 2 were considered. Typical diameters adopted for encased granular columns have been reported to range from 0.4 m to 1.0 m (Raithel et al., 2002, 2005; Alexiew et al., 2003; Araujo et al., 2009). For the diameter of the model column (0.15 m), the geometric scale factor of the models would then range from 2.7 to 6.7. In particular, assuming a prototype GEC having a diameter of 0.6 m, the

Table 2
Scale factors for laboratory large scale tests (Alkhorshid, 2017).

Dimensionless factor	Parameters	Scaling factor	Prototype	Model
$\pi_1 = \frac{T_g}{\rho.g.L.tg}$	T_g (kN/m)	λ^2 (=16)	500	31
$\pi_2 = \frac{J_g}{\rho.g.L.tg}$	J_g (kN/m)	λ^2 (=16)	2000	125
$\pi_3 = \frac{S_u}{\rho.g.L}$	S_u (kPa)	λ (=4)	< 20	< 5
$\pi_4 = \frac{D}{L}$	D (m)	λ (=4)	0.4–1	0.1–0.25

Where, Tg = Tensile strength, Jg = Tensile stiffness, ρ = the geosyntheic density, g = the gravity acceleration, L = Encasement length, tg = Encasement thickness, D = Column diameter.

corresponding scale factor (λ = prototype diameter/model diameter) would be equal to 4 (Table 2). The target value for the undrained shear strength of the manufactured soft soil was particularly small because of need of scaling such property. To achieve such low shear strength, the soil slurry was prepared with an approximate moisture content of 60% (the soil liquid limit) and allowed to consolidate under self-weight. This resulted in undrained strength values below 5 kPa (20 kPa under prototype conditions).

The GEC models were 150 mm in diameter and 1000 mm in height. Sand, calcareous gravel and recycled construction and demolition waste (RCDW) were used as fill materials for the columns. The particle size distributions of the sand, gravel and RCDW (mainly gravel and concrete) used to prepare the different models are also shown in Fig. 2. The use of RCDW in civil engineering construction has been recently encouraged as it is deemed environmentally friendly and may reduce project costs. However, the feasibility of its use should be verified, so an additional objective of the current research program was to assess its possible use in projects involving GECs. RCDW typically involves use of a variety of materials with varying dimensions. To achieve appropriate particle sizes for the dimensions of the models, only RCDW particles that passed the #3/4″ sieve were used. As indicated in Fig. 2, the RCDW particle size distribution was targeted at being very similar to that of the gravel, although their mechanical properties differed (Table 3). Relative density values of 82% for the sand and 85% for the gravel and RCDW were obtained after column preparation, which are consistent with values reported in the literature (Ali et al., 2012).

The values of peak friction angle, as obtained using a medium size (300 mm × 300 mm x 175 mm) direct shear box for the sand, gravel and RCDW were 41°, 43° and 42°, respectively, as obtained for normal stresses ranging from 50 kPa to 350 kPa. The relative density of the materials was equal to 82% for the sand and 85% for the gravel and RCDW. Dilatancy angles were estimated using the procedure reported by Bolton (1986) and the resulting values are given in Table 3. According to the USCS, the sand, gravel and RCDW are classified as SP, GP and GP, respectively.

Table 3
Properties of column materials.

Parameters	Sand	Gravel	RCDW
C_u (−)	3.51	1.6	1.5
C_c (−)	0.825	0.98	0.92
D_{50} (mm)	0.50	6.55	6.64
D_{10} (mm)	0.179	4.44	4.78
D_{30} (mm)	0.305	5.56	5.64
D_{60} (mm)	0.63	7.11	7.21
e_{max} (−)	0.87	0.74	0.76
e_{min} (−)	0.6	0.41	0.45
G_s	2.65	2.66	2.65
φ (°)	41	43	42
ψ (°)	11	12	12

Note: C_u = uniformity coefficient; C_c = coefficient of curvature; D_{10}, D_{30}, D_{50} and D_{60} = diameters of the soil particles for which 10, 30, 50 and 60% of the particles are finer, respectively; e_{max} and e_{min} = maximum and minimum void ratio, respectively; G_s = specific gravity; φ = friction angle; ψ = dilatancy angle.

Three types of woven geotextiles made of polyvinyl alcohol (labeled G-1) and polypropylene (labeled G-2 and G-3) were used for construction of the models. Because the diameter of the columns was 150 mm, encasement material of the required diameter was not commercially available. Consequently, the encasements were prepared using butterfly and flat seams. In the butterfly seam, as shown in Fig. 3, both edges of the geotextile are folded, with sewing being subsequently conducted. On the other hand, no folding was conducted on the edges for the case of the flat seam. Then the seam was tested in accordance with ASTM D4884/D4884M and the results are presented in Fig. 3 and Table 4. Since the stitched seam was weaker than the geotextile, failure developed at the location of the seam. Failure of the encasement was achieved, which was one of the objectives of this study. Evaluation of the evolution of the tests revealed that the seams did not significantly influence the uniformity of the cross-section other than at the location where failure took place after excessive bulging of the column.

2.3. Model column construction

To reach a target relative density of 85%, the model columns models were constructed in 200 mm thick layers. After preparation, the encased columns were placed in a 150 mm diameter PVC casing which was sealed at the tip by a geomembrane. Then, the pipe was subsequently pushed down into the soft soil until the column tip touched the bottom of the model tank. In order to keep the column perpendicular to the base of the box, a wood casing was utilized at the top. After completing the driving process, the PVC casing was carefully removed. Regarding heave, the authors did not notice relevant influence of the boundaries based both on visual inspection and on readings from instrumentation. It should be noted that the box dimensions are considerably larger than the column diameter (approximately 11 times). However, Alkhorshid (2017) provides figures illustrating the installation process as well as the heave after installation.

3. Experimental results

3.1. Load capacity of the model columns

For comparative purposes, conventional sand, gravel and RCDW model columns were also constructed and tested to serve as control. The performance of these columns was expected to be worse than that of the model GECs because of low lateral confinement. The three conventional columns tested as part of this study reached a very low load capacity, as shown by the load-settlement curves presented in Fig. 4(a–c).

The load-settlement curves for the encased sand column, shown in Fig. 4(a), clearly illustrate the importance of geotextile tensile stiffness and strength to column behavior. An increasing tensile strength (and stiffness) of the geotextile encasement was found to lead to an increasing load capacity and to a decreasing settlement of the corresponding model GEC. For instance, the mobilized load corresponding to a settlement of 50 mm (i.e. 5% of the column height) for G-1 was approximately twice that for G-2, and this ratio was essentially maintained throughout load capacity testing. The G-1 encased column (i.e. the column encased using geotextile G-1), which showed the highest tensile strength and stiffness among the geosynthetic products considered in this study, resulted in higher load capacity and lower settlement than the G-2 and G-3 encased columns.

Fig. 4(b) shows results from load capacity tests conducted on encased gravel columns. As expected, the results illustrate that the use of gravel in GEC construction led to an increased load bearing capacity than the use of sand. Comparison between the ultimate load capacity of encased gravel columns and that of sand columns reveals increases in the ultimate load capacity of 12%, 16.7% and 22.2% for G-1, G-2 and

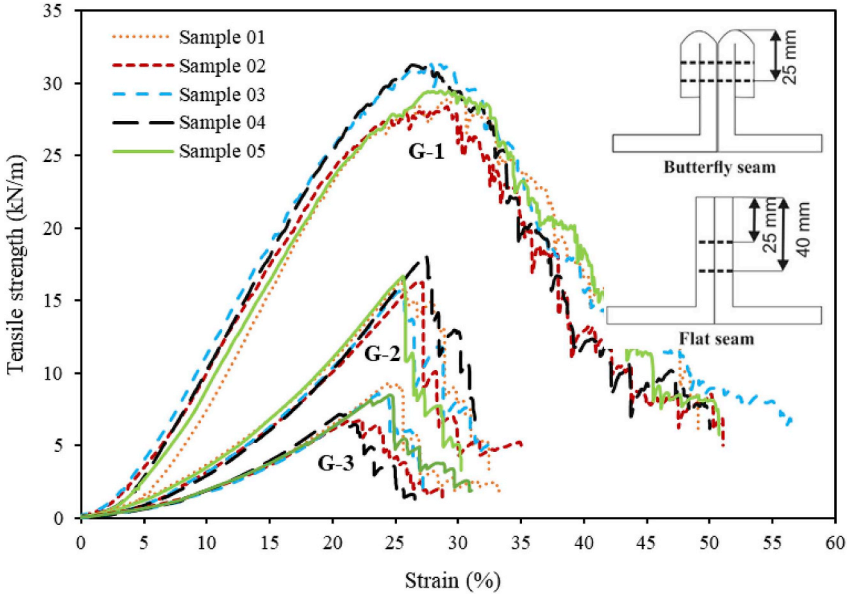

Fig. 3. Wide-width tensile tests of geotextile seam: G1 with butterfly seam; G2 with flat seam; G3 with flat seam.

Table 4
Mechanical properties of the geotextiles.

Properties	Geotextile Type		
	G-1 (Butterfly seam)	G-2 (Flat Seam)	G-3 (Flat Seam)
Maximum tensile strength of seam (kN/m)	30	16	8
Strain at maximum tensile strength (%)	22	16	15
Stiffness at 5% strain (kN/m)	120	107	53.4

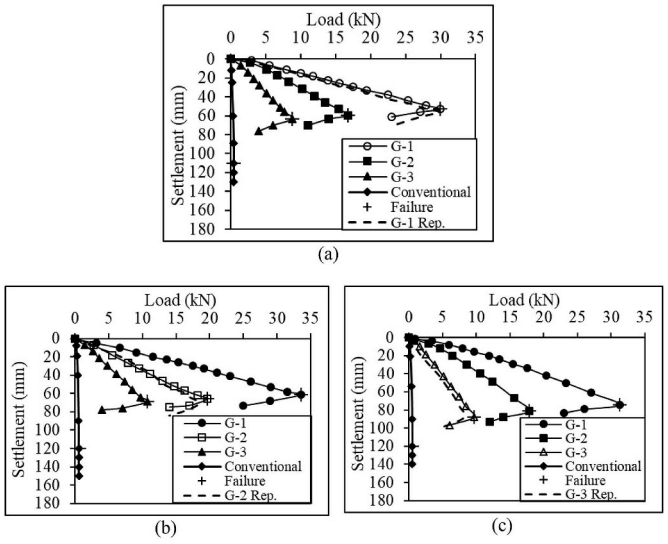

Fig. 4. Load-settlement response: (a) sand columns; (b) gravel columns; (c) RCDW columns.

G-3, respectively. In addition, the settlement obtained at ultimate load capacity for the G-1 encased gravel column was approximately 15% higher than that of the G-1 encased sand column. Similarly, the settlements at ultimate load capacity for the G-2 and G-3 encased gravel columns were 10.9% and 9.5% higher than those for the corresponding encased sand columns, respectively. The higher settlements reached for the gravel columns can be attributed to the breakage of gravel particles, as will be discussed in Section 3.6 of this paper. The repeatability of the load-settlement results was corroborated by the results of three tests: G-1 Rep, G-2 Rep and G-3 Rep. The results from these three repeats are presented in Fig. 4(a), (b) and 4(c), respectively.

The results presented in Fig. 4(c) indicate that the load mobilized on the encased RCDW column for a settlement of 50 mm, for a given geotextile type, was found to be smaller than that obtained for the corresponding encased sand. Fig. 5 summarizes the load values mobilized for a settlement of 50 mm for each of the 12 model columns tested as part of this investigation. The results presented in this figure indicate only slight differences among the results for the three fill aggregate materials used to construct the columns. However, the magnitude of the load mobilized in the encased RCDW columns was found to be consistently smaller than that mobilized in the encased sand and gravel columns for the three geotextiles used in this study.

The settlement of the RCDW encased column was up to 40% greater than that of the sand column at ultimate load capacity. Larger settlements were also observed when RCDW was used for G-2 and G-3 (36%

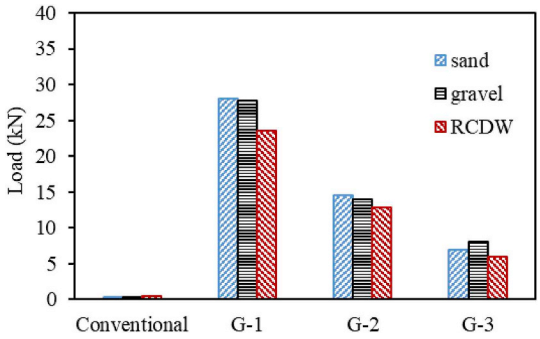

Fig. 5. Column loads mobilized for a settlement of 50 mm (5% of column height).

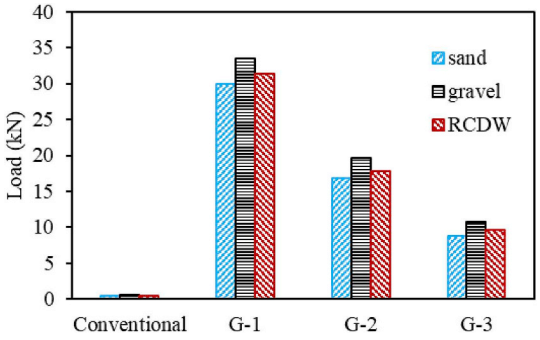

Fig. 6. Column ultimate load capacity values.

and 40%, respectively). These large settlements are associated with breakage of the RCDW particles, which will be discussed later in the paper.

Fig. 6 presents the ultimate load capacity for each model column tested as part of this study. It should be noted that the same failure mechanism (encasement failure) occurred in the nine GEC models. The conventional columns resisted only very low ultimate loads as compared to the encased columns. For example, the ultimate load capacity of the conventional sand columns was increased by factors of 71, 40 and 21 if the columns were encased using geotextiles G-1, G-2 and G-3, respectively. Since G-1 was the geotextile with the highest tensile strength and stiffness values among those used in this study, the load capacity increase was higher than those of G-2 and G-3. These results confirm the significant benefits in terms of ultimate load capacity of using encasement to improve the mechanical properties of otherwise conventional columns.

3.2. Lateral bulging of the model columns

After the load capacity tests were completed, the sand columns were carefully exhumed to measure the lateral bulging along its entire length. The fill material in the columns was excavated until reaching half of the column length, and the cavity was subsequently filled with plaster and left to rest for 24 h.

The maximum bulging in the columns was quantified by measuring the increase in maximum column diameter in the exhumed models and quantifying the maximum radial strains Evaluation of these results indicate that the maximum lateral bulging in the G-1 encased column was 11.34% (in terms of radial strain) at a depth of about 150–180 mm below the soil surface (Fig. 7(a)). The depth below the soil surface over which bulging occurred was approximately twice the footing width. While little bulging was noted somewhat uniform radial strains were observed below a depth of about 300 mm. The measured bulging and overall measurement of radial strains are in agreement with results reported by Greenwood (1970), Hughes et al. (1975) and Hong et al. (2016), in their field and laboratory studies, respectively, who reported column bulging over depths below four times the column diameter.

Comparatively more pronounced bulging was observed in the G-2 and G-3 encased columns, as the geotextiles in these models have a lower stiffness than G-1 (Fig. 7(b and c)). The largest radial strain (12.5%) occurred in the G-3 encased column (Fig. 7(c)). However, the depth over which bulging occurred was similar to that of the G-1 encased column.

The increase in radial strains can be used with the geotextile tensile stiffness to predict the ring tensile forces acting on the column encasement. The maximum ring tensile force was observed to occur at approximately the same depth for the sand columns encased with any of the three geotextile types used in this study. The representative results in Fig. 8 show the ring tensile force along the column height, also showing that the maximum ring force in each column occurred at the

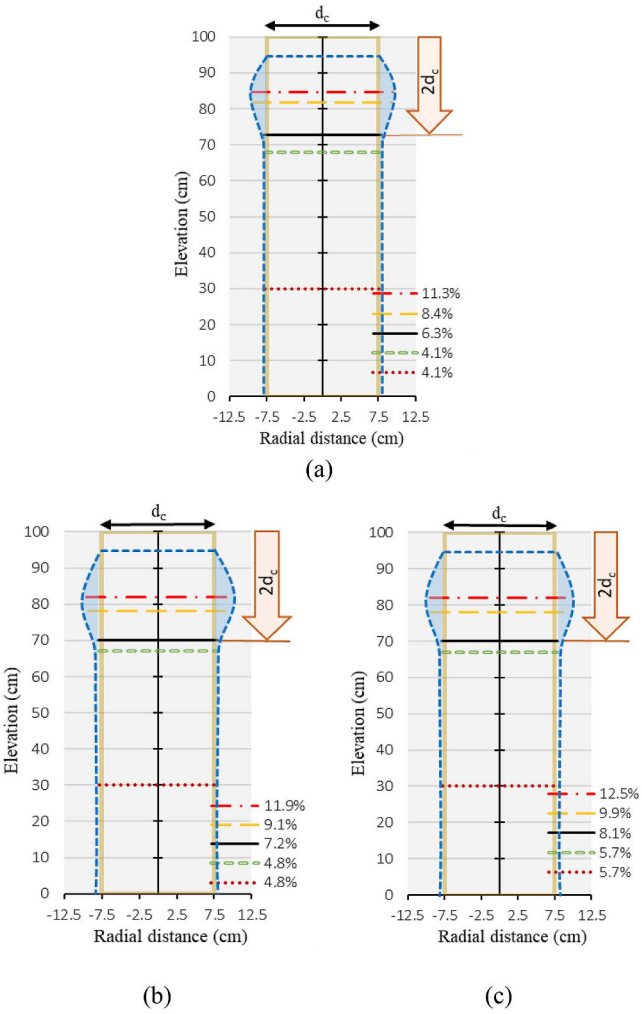

Fig. 7. Bulging and radial strains at different depths for encased sand columns: (a) G-1 encased column; (b) G-2 encased column; (c) G-3 encased column.

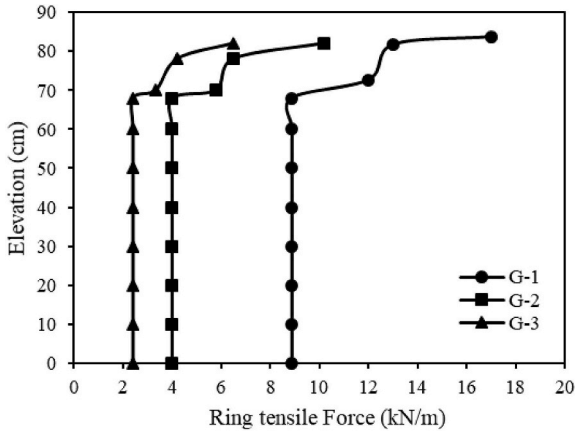

Fig. 8. Ring tensile force distribution versus sand column elevation.

points of maximum bulging. The ring force remained relatively constant throughout the column height below the region where bulging was more pronounced. A comparison of the seam tensile strength of each geotextile (Table 4) with the maximum ring tensile force reached in the corresponding encased column (Fig. 8) indicate that 43%, 36% and 19% of the seam tensile strength was mobilized at the time of failure in

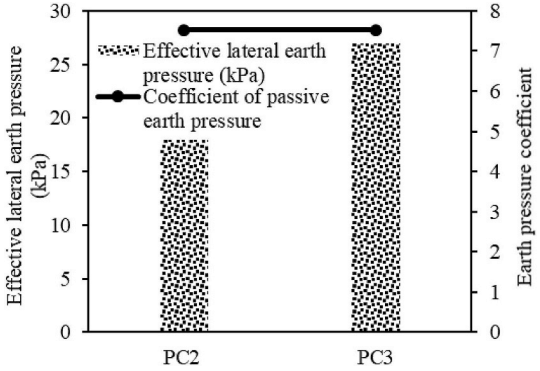

Fig. 9. Effective lateral earth pressures generated immediately after column installation, along with magnitude of lateral earth pressure coefficients.

the G-1, G-2 and G-3 encased columns, respectively. These differences can be due to different mechanical properties of the geotextiles used as encasement and also to the column behavior after failure. Even after failure, the encasement tends to regain much of its initial condition upon unloading of the column, causing some reduction in the column bulging and consequently a decrease in the ring tensile forces.

3.3. Lateral earth pressures

Three pressure cells were installed at different depths along the side of the column. Since the columns were installed using the displacement method, the soil was therefore displaced toward the pressure cells during installation. Exhumation of the columns after the testing showed that, in general, PC1 and PC2 showed a horizontal displacement of approximately 20 mm from their original locations. On the other side of the column, P1, P3 and P6 showed a horizontal displacement of approximately 10 mm. Finally, P2, P4 and P5 showed no displacement in relation to their original position. In addition, pore water pressures were estimated at the locations of PC2 and PC3 using the readings collected from piezometers. Based on the locations of piezometers, the pore pressure changes were calculated along both the vertical and horizontal directions. The effective lateral earth pressures were then predicted by subtracting pore pressures from the total lateral pressures. Fig. 9 shows the maximum effective lateral pressures, predicted immediately after column installation, at the location of sensors PC2 and PC3. The predicted values for the coefficient of lateral earth pressure at each elevation are also presented in the figure, indicating that it reached the magnitude of 7.5.

Since the maximum bulging occurred at a depth of approximately 160 mm, only PC1 was affected by column bulging and no output was registered for PC2 and PC3 during the loading phases. The effective lateral pressures obtained for the G-2 encased column were greater than those for the G-1 encased column, as the G-2 encased column presented greater lateral bulging. Consequently, the maximum coefficient of lateral earth pressure obtained for the G-2 encased column was higher than that for the G-1 encased column (Fig. 10).

The lateral earth pressures acting against the encasement were found to reach the value corresponding to the passive condition, as shown by the magnitude of the Rankine passive lateral earth pressure coefficient, shown in the figure as reference. Priebe (1976) and Gäb et al. (2008) reported that the coefficient of lateral earth pressure after installation can be assumed to be K = 1 for design purposes. On the other hand, Baumann and Bauer (1974) assumed the lateral earth pressures can be assumed considering a lateral earth pressure coefficient ranging from its at-rest to its passive values. Based on the results of this study, the values obtained for lateral earth pressure during loading tests are reasonably high, reaching values consistent with the passive condition.

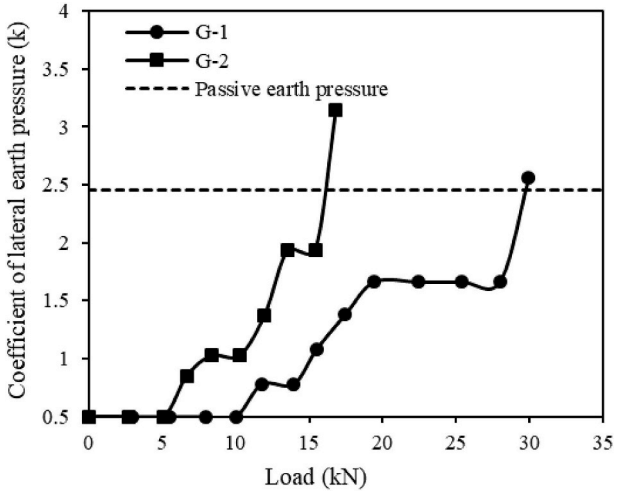

Fig. 10. Coefficient of lateral earth pressures obtained at the elevation of sensor PC1 in sand columns.

3.4. Excess pore water pressures

Six piezometers were positioned at different depths and varying radial distances from the column (Fig. 1) to monitor changes in excess pore water pressure during installation and load capacity testing of the model columns. Initial measurements recorded values equal to the hydrostatic pore pressures, confirming the saturated condition of the soft soil. Excess pore water pressures within the soil were found to be primarily generated during construction, which involved the displacement method. Thus, the excess pore water pressure measurements obtained during column driving were reasonably similar for both encased and conventional columns. The results presented in Fig. 11 show the dissipation of excess pore water pressure after installation of the G-1 encased sand column. A sharp increase in excess pore pressures can be observed in the figure, for all piezometers, due to the driving of the PVC casing, which occurred over approximately 43 h. The figure also shows the subsequent dissipation of excess pore water pressures, which can be observed to occur up to approximately 43 h after column installation. The maximum excess pore water pressure value was registered immediately after installation by P1, located at the bottom of the box and in close radial distance to the column. The minimum value immediately after installation was registered by P6, which was at a comparatively shallow depth from the soil surface (drainage boundary). No changes in pore pressures were recorded by P5, which was located at a radial distance of approximately 450 mm ($\approx 3d_c$) from the column. The results therefore indicate that column installation generated excess pore water pressures up to a distance equivalent to three column diameters.

Piezometers P1 and P2 registered comparatively high excess pore pressures and required the longest amount of time for full dissipation. This response is consistent with the drainage conditions. No significant changes were observed in the values of excess pore water pressure during subsequent loading stages.

3.5. Undrained shear strength

Tests were conducted to characterize the in-situ undrained shear strength of the soft soil at varying distances from the column. The tests involved use of a laboratory vane shear test apparatus. The tests were conducted before column installation, immediately after their installation and after full dissipation of excess pore water pressures generated within the soil mass due to column installation. The vane tests were carried out at radial distances of 30, 60 and 90 mm (Fig. 12) for depths of 200, 400, 600 and 800 mm.

Fig. 12 depicts the undrained shear strength values obtained after

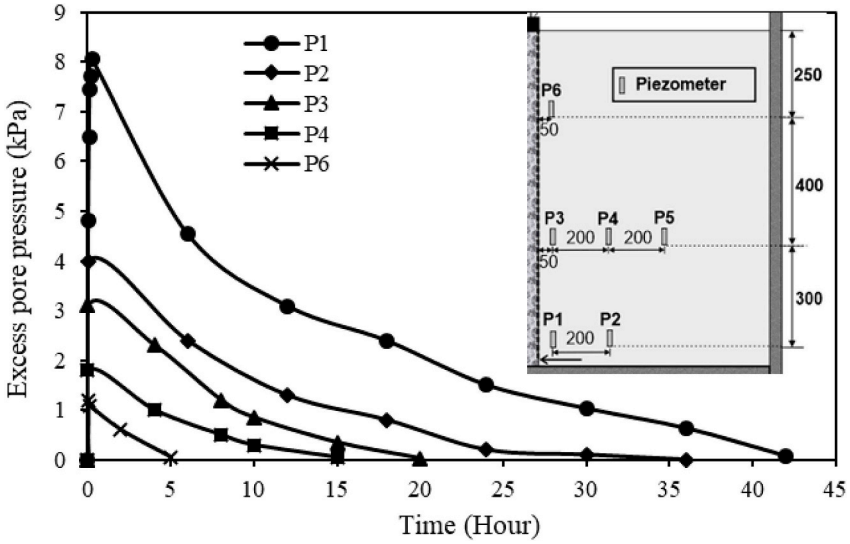

Fig. 11. Dissipation of excess pore water pressure.

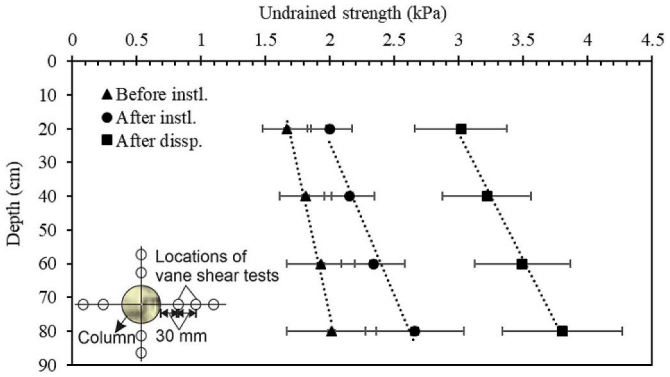

Fig. 12. Undrained shear strength results along the columns' depth at different stages after column installation.

correction of the test results using the procedure reported by Bjerrum (1972). Series of six vane shear tests were conducted for each of the encased and conventional (non-encased) columns at a radial distance of 30 mm from the column. The standard deviation for each set of tests is also plotted in this figure. Based on the results, it can be inferred that the precision of the vane shear tests may decrease with increasing depth. The shear strength results obtained from vane shear tests conducted at radial distances of 60 and 90 mm from the column were similar to those obtained before the column installation.

The results in Fig. 12 show that the dissipation of excess pore water pressures resulted in increased undrained shear strength of the soft soil after column installation. Specifically, the undrained shear strength was found to increase by 200% in relation to the values obtained before column installation. Raithel et al. (2002) reported that after installation of encased columns, the undrained shear strength of the adjacent soils increased up to 300%. However, the authors did not specify whether the tests were conducted immediately after the column installation or at a later time.

3.6. Breakage of gravel and RCDW particles

The fill materials of the gravel and RCDW columns were sieved after the loading test to evaluate the extent of particle breakage. To facilitate this evaluation, particle breakage was assessed along five 150-mm thick segments of the column height (Fig. 13). The particle breakage index (B_g), as proposed by Marsal (1967), was calculated for each segment.

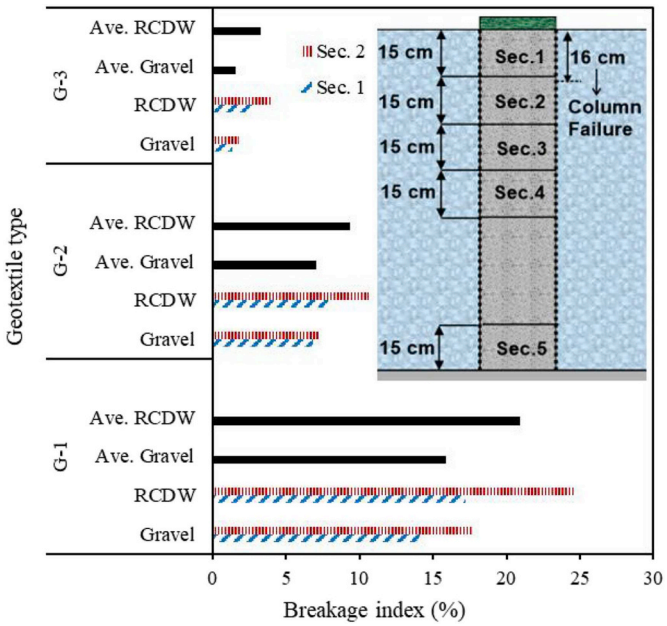

Fig. 13. Breakage index obtained using fill material retrieved from the gravel and RCDW columns.

The test results from tests conducted using fill material from Sections 1 and 2 (top 300 mm of the column) before the load test showed differences in relation to test results conducted using the material retrieved after load testing. On the other hand, the results from tests conducted using fill material from Sections 3, 4 and 5 did not show any significant differences. Fig. 13 shows the particle breakage index obtained for fill material from Sections 1 and 2. B_g values for both gravel and RCDW columns were greater for Section 2 than for Section 1. It should be noted that encasement failure took place within Section 2. The higher B_g values obtained for RCDW columns may be attributed to the heterogeneity of the material.

The particle breakage index for fill material retrieved from the G-3 encased column (geotextile with the lowest tensile stiffness) was below 4% for both the gravel and RCDW columns. On the other hand, comparatively high B_g values were obtained for fill material retrieved from the G-1 encased column, which is consistent with the comparatively higher confinement provided by the encasement in this case. Therefore, the encasement tensile stiffness may influence B_g values of column fill

materials and consequently column settlement and load capacity.

3.7. Comparisons between predicted and measured results: ultimate load capacity and encasement tensile strength

Briaud (2013) presented an analytical method to predict the load bearing capacity of a single encased column. This method takes into account the influence of the geosynthetic tensile stiffness and the elevation of the water table to estimate the bearing capacity of the column. Based on the method the ultimate load capacity of the encased column can be calculated by the following equation:

$$P_u = k_p(P'_L + P_{geo}) \quad (1)$$

where, k_p is passive earth pressure of the column material ($k_p = \frac{1+\sin\varphi}{1-\sin\varphi}$), P'_L is effective stress and P_{geo} is the pressure contributed by the encasement obtained by:

$$P_{geo} = E\frac{\Delta r}{r_0^2} \quad (2)$$

where, E, Δr and r_0 are geotextile tensile stiffness, radius variation and initial radius of the column, respectively.

Van Impe and Silence (1986) and Raithel and Kempfert (2000) proposed analytical methods to predict the tensile strength of an encasement considering the vertical stress on the column. Both methods consider active earth pressures acting on the column, as they assume that the column reaches an active condition when approaching failure.

The ultimate load capacity of each of the nine columns evaluated in this study was predicted using the procedure reported by Briaud (2013). Fig. 14(a) shows that a particularly good comparison could be achieved between the measured and predicted ultimate load capacity for each encased column evaluated as part of this study. More specifically, the analytical method was found to slightly overpredict the measured ultimate load capacity for the case of the encased gravel and RCDW columns, while it accurately predicted the measured ultimate load capacity for the case of the encased sand columns.

Fig. 14(b) shows a comparison between predicted values of ring tensile forces in the geotextile encasement at failure, as proposed by Van Impe and Silence (1986 – code VI&S) and Raithel and Kempfert (2000 – code R&K), and measured values of tensile strength (maximum tensile strength of seam). The maximum vertical stress on top of the column was used to predict the tensile force in the geotextile encasement according to these two methods. In Raithel and Kempfert (2000), the maximum load on the column from the tests was used that could be considered as a particular case in which the efficiency of the column is approximately 100%. In general, predictions and measurements compared well, with slight underpredictions for G-1 and G2. It should be pointed out that the good agreement between the predictions obtained via the simple method by Van Impe and Silence (1986) and measurements may to some extent be related to the testing conditions of the model columns, which more closely satisfy the assumptions of this method. Column properties and vertical stress are vital for the prediction of encasement tensile strength in these analytical methods. However, in the method proposed by Raithel and Kempfert (2000) the soil parameters can influence the predictions very slightly. The soft soil parameters used in the predictions conducted as part of this study are presented in Table 5.

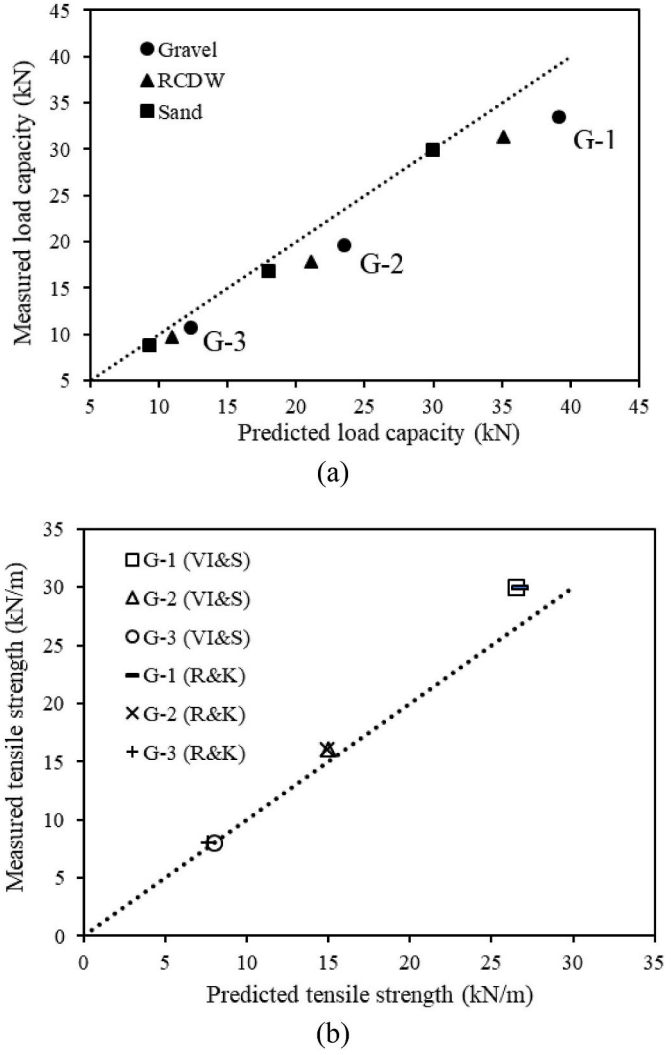

Fig. 14. Comparison between predicted and measured values: (a) load capacity for columns constructed using different geotextiles; and (b) tensile strength reached in different geotextiles used as column encasement.

Table 5
Soft soil parameters for $S_u < 5$ kPa (Raithel and Kempfert, 2000).

Soil parameters	Value
Friction angle (°)	25
Poisson's ratio (−)	0.4
Unit weight (kN/m^3)	17
Oedometric modulus (kPa)	725

4. Conclusions

The behavior of geotextile encased and conventional granular columns placed in very soft soils was evaluated in this study through load capacity tests conducted on large-scale laboratory model columns. The encased columns were constructed using three different types of fill material and three different geotextile materials. The following conclusions can be drawn based on the results obtained in this investigation:

- The three geotextile types used as encasement in this study provided a significant increase in load capacity as compared to conventional columns. For example, the tests involving sand columns revealed that use of geotextile encasement led to an increase in ultimate load capacity of 7121%, 4000% and 2100% for the G-1, G-2 and G-3 encased columns, respectively.
- The breakage indices (B_g) calculated for gravel and RCDW materials revealed that increased stress affected the column fill materials up to a depth of approximately twice the column diameter. Therefore, the core material's shear strength in this zone is of particular importance. The influence of particle breakage on the ultimate and

serviceability limit states of GECs should be accounted for in design.

- The maximum lateral bulging of the encased columns occurred for the column encased with the weakest geotextile (G-3) at a depth ranging from 1 to 1.5 times the column diameter. The location of maximum bulging was approximately the same for all encasement types.
- Evaluation of the lateral earth pressure data revealed that a reasonably uniform lateral earth pressure with depth should be expected during column installation. On the other hand, the increase in lateral earth pressures during load capacity is expected to occur only within an approximate depth of 1–2 times the column diameter.
- The diameter of the smear zone measured about 1.8–1.9 times the column diameter (d_c) since the vane shear tests out of this zone did not present any improvement in the soil shear strength. In addition, the results of vane shear tests in this zone did not show significant variability in the soil undrained shear strength before dissipation of the excess pore water pressures. On the other hand, the undrained shear strength within the smear zone was found to increase up to twice its initial value after dissipation of pore water pressures.
- Generation of excess pore water pressures was observed during the column installation stage. However, but no further significant increase was noted during subsequent loading stages.
- The column ultimate load capacity predicted using the analytical method proposed by Briaud (2013) was found to agree well with measured results. Also, the geotextile tensile strength predicted using approaches proposed by Van Impe and Silence (1986) and Raithel and Kempfert (2000) were found to compare satisfactorily with measurements.

Acknowledgments

The authors would like to thank the following institutions for their support in the research activities described in this paper: Brazilian National Council for Scientific and Technological Development (CNPq), CAPES-Brazilian Ministry of Education, University of Brasília, Federal University of Itajuba and INFRALAB and Huesker Geosynthetics.

References

ABNT, 2000. NBR 14545: Solo – Determinção do coeficiente de permeabilidade de solos argilosos a carga variável. 12pp., Rio de Janeiro.

Alexiew, D., Raithel, M., 2015. Geotextile-encased columns: case studies over twenty years. In: Indraratna, Em B., Chu, J., Rujikiatkamjorn, C. (Eds.), Ground Improvement Case Histories. Elsevier, Kidlington, Oxford, pp. 451–477. https://doi.org/10.1016/B978-0-08-100192-9.00017-X.

Alexiew, D., Horgan, G.J., Brokemper, D., 2003. Geotextile encased column (GEC): load capacity and geotextile selection. In: In Foundations: Innovations, Observations, Design and Practice, . https://doi.org/10.1061/40777(156)12.

Ali, K., Shahu, J.T., Sharma, K.G., 2012. Model tests on geosynthetic-reinforced stone columns: a comparative study. Geosynth. Int. 19 (4), 433–451. https://doi.org/10.1680/gein.12.00016.

Ali, K., Shahu, J.T., Sharma, K.G., 2014. Model tests on single and groups of stone columns with different geosynthetic reinforcement arrangement. Geosynth. Int. 21 (2), 103–118. https://doi.org/10.1680/gein.14.00002.

Alkhorshid, N.R., 2012. Numerical Analysis of Soft Clay Reinforced with. Eastern Mediterranean University, Gazimağusa, North Cyprus.

Alkhorshid, N.R., 2017. Analysis of Geosynthetic Encased Columns in Very Soft Soil. PhD Thesis, 128 P, G.TD-133/17. University of Brasilia, Department of Civil and Environmental Engineering, Brasilia.

Alkhorshid, N.R., Araújo, G.L., Palmeira, E.M., 2018. Behavior of geosynthetic-encased stone columns in soft clay: numerical and analytical evaluations. Soils and Rocks 41 (3), 333–343. https://doi.org/10.28927/SR.413333.

Alkhorshid, N.R., Nalbantoglu, Z., Araujo, G.L., 2014. 3D analysis of full scale stone column reinforced soft clay: numerical evaluation. In: XVII Congresso Brasileiro de Mecânica dos. Cobramseg, Goiânia.

Almeida, M.S.S., Hosseinpour, I., Riccio, M., 2013. Performance of a geosynthetic-encased column (GEC) in soft ground: numerical and analytical studies. Geosynth. Int. 20 (4), 252–262. https://doi.org/10.1680/gein.13.00015.

Araujo, G.L., Palmeira, E.M., Cunha, R.P., 2009. Behaviour of geosynthetic-encased granular columns in porous collapsible soil. Geosynth. Int. 16 (6), 433–451. https://doi.org/10.1680/gein.2009.16.6.433.

ASTM(D4884/D4884M), 2014. Standard Test Method for Strength of Sewn or Bonded Seams of Geotextiles. ASTM International, West Conshohocken. https://doi.org/10.1520/D4884_D4884M-14A.

ASTM(D5084), 2016. Standard Test Methods for Measurement of Hydraulic Conductivity of Saturated Porous Materials Using a Flexible Wall Permeameter. Originally approved in 1990. ASTM International, West Conshohocken, PA 19428-2959. United States. https://doi.org/10.1520/D5084-16A.

Baumann, V., Bauer, G.E., 1974. The performance of foundations on various soils stabilized by the vibro-compaction method. Can. Geotech. J. 11 (4), 509–530. https://doi.org/10.1016/0148-9062(75)90103-5.

Bjerrum, L., 1972. Embankments on soft ground. In: Proceedings of the ASCE Conference on Performance of Earth-Supported, pp. 1–54.

Bolton, M.D., 1986. The strength and dilatancy of sands. Geotechnique 36 (1), 65–78. https://doi.org/10.1680/geot.1986.36.1.65.

Briaud, J.L., 2013. Geotechnical Engineering: Unsaturated and Saturated Soils. John Wiley & Sons, Hoboken, New Jersey.

Castro, J., Sagaseta, C., 2011. Deformation and consolidation around encased stone columns. Geotext. Geomembranes 29 (3), 268–276. https://doi.org/10.1016/j.geotexmem.2010.12.001.

Chen, J., Li, L., Xue, J., Feng, S., 2015. Failure mechanism of geosynthetic-encased stone columns in soft soils under embankment. Geotext. Geomembranes 43 (5), 424–431. https://doi.org/10.1016/j.geotexmem.2015.04.016.

Cimentada, A., Da Costa, A., Cañizal, J., Sagaseta, C., 2011. Laboratory study on radial consolidation and deformation in clay reinforced with stone columns. Can. Geotech. J. 48 (1), 36–52. https://doi.org/10.1139/T10-043.

Dash, S.K., Bora, M.C., 2013. Influence of geosynthetic encasement on the performance of stone columns floating in soft clay. Can. Geotech. J. 50 (7), 754–765. https://doi.org/10.1139/cgj-2012-0437.

De Mello, L.G., Mondolfo, M., Montez, F., Tsukahara, C.N., Bilfinger, W., 2008. First use of geosynthetic encased sand columns in South America. In: Proceedings of 1st Pan-American Geosynthetics Conference, pp. 1332–1341.

Elsawy, M.B., 2013. Behaviour of soft ground improved by conventional and geogrid-encased stone columns, based on FEM study. Geosynth. Int. 20 (4), 276–285. https://doi.org/10.1680/gein.13.00017.

Fattah, M.Y., Zabar, B.S., Hassan, H.A., 2016. Experimental analysis of embankment on ordinary and encased stone columns. Int. J. Geomech. 16 (4) 04015102. https://doi.org/10.1061/(ASCE)GM.1943-5622.0000579.

Gäb, M., Schweiger, H.F., Kamrat-Pietraszewska, D., Karstunen, M., 2008. Numerical analysis of a floating stone column foundation using different constitutive models. In: Second International Workshop on Geotechnics of Soft Soils. CRC Press, glasgow, scotland, pp. 137–142 3–5 september.

Geng, L., Tang, L., Cong, S.Y., Ling, X.Z., Lu, J., 2017. Three-dimensional analysis of geosynthetic-encased granular columns for liquefaction mitigation. Geosynth. Int. 24 (1), 45–59. https://doi.org/10.1680/jgein.16.00014.

Ghazavi, M., Afshar, J.N., 2013. Bearing capacity of geosynthetic encased stone columns. Geotext. Geomembranes 38, 26–36. https://doi.org/10.1016/j.geotexmem.2013.04.003.

Gniel, J., Bouazza, A., 2009. Improvement of soft soils using geogrid encased stone columns. Geotext. Geomembranes 27 (3), 167–175. https://doi.org/10.1016/j.geotexmem.2008.11.001.

Greenwood, D.A., 1970. Mechanical improvement of soils below ground surface. In: Proceedings of Conference on Ground Engineering. Institution of Civil Engineers, London, pp. 11–22.

Gu, M., Zhao, M., Zhang, L., Han, J., 2016. Effects of geogrid encasement on lateral and vertical deformations of stone columns in model tests. Geosynth. Int. 23 (2), 100–112. https://doi.org/10.1680/jgein.15.00035.

Hong, Y.-S., Wu, C.-S., Yu, Y.-S., 2016. Model tests on geotextile-encased granular columns under 1-g and undrained conditions. Geotext. Geomembranes 44 (1), 13–27. https://doi.org/10.1016/j.geotexmem.2015.06.006.

Hosseinpour, I., Riccio, M., Almeida, S., 2015. Full-scale load test and finite-element analysis of soft ground improved by geotextile-encased granular columns. Geosynth. Int. 22 (6), 428–438. https://doi.org/10.1680/jgein.15.00023.

Hughes, J.M., Withers, N.J., Greenwood, D.A., 1975. A field trial of the reinforcing effect of a stone column in soil. Geotechnique 25 (1), 31–44. https://doi.org/10.1680/geot.1975.25.1.31.

Kaliakin, V.N., Khabbazian, M., Meehan, C.L., 2012. Modelling the behavior of geosynthetic encased columns: influence of granular soil constitutive model. Int. J. Geomech. 12 (4), 357–369. https://doi.org/10.1061/(ASCE)GM.1943-5622.0000084.

Keykhosropur, L., Soroush, A., Imam, R., 2012. 3D numerical analyses of geosynthetic encased stone columns. Geotext. Geomembranes 35, 61–68. https://doi.org/10.1016/j.geotexmem.2012.07.005.

Khabbazian, M., Kaliakin, V.N., Meehan, C.L., 2010. Numerical study of the effect of geosynthetic encasement on the behaviour of granular columns. Geosynth. Int. 17 (3), 132–143. https://doi.org/10.1680/gein.2010.17.3.132.

Marsal, R., 1967. Large scale testing of rockfill materials. J. Soil Mech. Found. Div. ASCE 27–43.

Mazumder, T., Rolaniya, A.K., Ayothiraman, R., 2018. Experimental study on behaviour of encased stone column with tyre chips as aggregates. Geosynth. Int. 25 (3), 259–270. https://doi.org/10.1680/jgein.18.00006.

McCabe, B.A., Nimmons, G.J., Egan, D., 2009. A review of field performance of stone columns in soft soils. Proc. Inst. Civ. Eng.- Geotech. Eng. 162 (6), 323–334. https://doi.org/10.1680/geng.2009.162.6.323.

Miranda, M., Da Costa, A., Castro, J., Sagaseta, C., 2015. Influence of gravel density in the behaviour of soft soils improved with stone columns. Can. Geotech. J. 52 (12), 1968–1980. https://doi.org/10.1139/cgj-2014-0487.

Mohapatra, S.R., Rajagopal, R., Sharma, J., 2017. 3-Dimensional numerical modeling of

geosynthetic-encased granular columns. Geotext. Geomembranes 45 (3), 131–141. https://doi.org/10.1016/j.geotexmem.2017.01.004.
Murugesan, S., Rajagopal, K., 2007. Model tests on geosynthetic-encased stone columns. Geosynth. Int. 14 (6), 346–354. https://doi.org/10.1680/gein.2007.14.6.346.
Murugesan, S., Rajagopal, K., 2009. Investigations on the behavior of geosynthetic encased stone columns. In: Proc. Of the 17th ICSMGE. Alexandrina, Egypt.
Noor Muneerah PG Haji Jeludin, D.K., Sivakumar, V., O'Kelly, B.C., Mackinnon, P.A., 2015. Experimental observations of settlement of footings supported on soft clay reinforced with granular columns: laboratory model study. J. Geotech. Geoenviron. Eng. 142 (1) 04015063. https://doi.org/10.1061/(ASCE)GT.1943-5606.0001377.
Ou Yang, F., Zhang, J.J., Liao, W.M., Han, J.W., Tang, Y.L., Bi, J.B., 2017. Characteristics of the stress and deformation of geosynthetic-encased stone column composite ground based on large-scale model tests. Geosynth. Int. 24 (3), 242–254. https://doi.org/10.1680/jgein.16.00028.
Priebe, H.J., 1976. Evaluation of the settlement reduction of a foundation improved by Vibro-replacement. Bautechnik 2, 160–162 (in German).
Pulko, B., Majes, B., Logar, J., 2011. Geosynthetic-encased stone columns: analytical calculation model. Geotext. Geomembranes 29 (1), 29–39. https://doi.org/10.1016/j.geotexmem.2010.06.005.
Raithel, M., Kempfert, H.G., 2000. Calculation models for dam foundations with geotextile coated sand columns. In: Proceeding of the International Conference on Geotechnical and Geological Engineering. Melbourne.
Raithel, M., Kempfert, H.G., Kirchner, A., 2002. Geotextile-encased columns (GEC) for foundation of a dyke on very soft soils. In: Proceedings of the Seventh International Conference on Geosynthetics, pp. 1025–1028.
Raithel, M., Kirchner, A., Schade, C., Leusink, E., 2005. Foundation of construction on very soft soils with geotextile encased columns. state of the art. In: Proceedings of GeoFrontiers 2005. Austin, Texas.
Rajesh, S., 2017. Time-dependent behaviour of fully and partially penetrated geosynthetic encased stone columns. Geosynth. Int. 24 (1), 60–71. https://doi.org/10.1680/jgein.16.00015.
Rayamajhi, D., Boulanger, R.W., Ashford, S.A., Elgamal, A., 2016. Dense granular columns in liquefiable ground. II: effects on deformations. J. Geotech. Geoenviron. Eng. 142 (7) 04016024. https://doi.org/10.1061/(ASCE)GT.1943-5606.0001475.
Schnaid, F., Winter, D., Silva, A.E., Alexiew, D., Kuster, V., 2017. Geotextile encased columns (GEC) used as pressure-relief system. Instrumented bridge abutment case study on soft soil. Geotext. Geomembranes 45 (3), 227–236. https://doi.org/10.1016/j.geotexmem.2017.02.003.
Shahu, J.T., Reddy, Y.R., 2014. Estimating long-term settlement of floating stone column groups. Can. Geotech. J. 51 (7), 770–781. https://doi.org/10.1139/cgj-2012-0477.
Van Impe, W.F., Silence, P., 1986. Improving of the bearing capacity of weak hydraulic fills by means of geotextiles. In: 3rd Inernational Conference on Geosynthetics, vol. 5. pp. 1411–1416 Vienna, Austria.
Xu, C., Song, S., Han, J., 2016. Scaled model tests on influence factors of full geosynthetic-reinforced pile-supported embankments. Geosynth. Int. 23 (2), 140–153. https://doi.org/10.1680/jgein.15.00038.
Xue, J., Liu, Z., Chen, J., 2019. Triaxial compressive behaviour of geotextile encased stone columns. Comput. Geotech. 108, 53–60. https://doi.org/10.1016/j.compgeo.2018.12.010.
Zhang, Y., Li, T., Wang, Y., 2011. Theoretical elastic solutions for foundations improved by geosynthetic-encased columns. Geosynth. Int. 18 (1), 12–20. https://doi.org/10.1680/gein.2011.18.1.12.